



Maximum Likelihood Classification of Single High-resolution Polarimetric SAR Images in Urban Areas

MARYAM SOHEILI MAJD, ELISABETH SIMONETTO & LAURENT POLIDORI, Le Mans, France

Keywords: PolSAR, urban area, supervised classification, maximum likelihood

Summary: In this work, our aim is to assess the potential of a single polarimetric radar image of high spatial resolution for the classification of urban areas. For that purpose, we concentrate on a fine definition of urban land cover types including ground classes corresponding to different roof types and we test several supervised classification algorithms. In particular, we deal with maximum likelihood classification using several polarimetric and textural indices. At first, we propose a state-of-the-art statistical analysis of polarimetric synthetic aperture radar (SAR) data to study the statistical behaviours of these indices. We consider the Gauss, log-normal, Beta 1, Weibull, Gamma, K, and Fisher statistical models and estimate their parameters using two methods: maximum likelihood estimation (MLE), and method of log-moment (MoLM). The Fisher probability density function (pdf) is able to properly model all the descriptors. Then, we propose to introduce this information in an adapted supervised classification scheme based on maximum likelihood and the Fisher pdf. We compare the classification results with the Wishart-based maximum likelihood algorithm, a Gaussian-based one and SVM (support vector machine). Our experiments are based on an image of a suburban area, acquired by the airborne RAMSES SAR sensor of ONERA, the French Aerospace Lab. The results highlight the potential of such data to discriminate urban land cover types, and the overall accuracy reaches 84%. However, the results from the tested classification methods show a problematic confusion between roofs and trees. Some possible solutions are discussed at the end of this paper.

Zusammenfassung: Ziel dieser Arbeit ist es, das Potenzial eines einzelnen hoch aufgelösten polarimetrischen Radar-Bildes für die Klassifikation von urbanen Gebieten zu testen. Zu diesem Zweck zielen wir auf eine feine Unterscheidung von urbanen Landbedeckungsarten mit mehreren Objektklassen, die unter anderem auch verschiedenen Arten von Dächern entsprechen, und wir testen verschiedene überwachte Klassifikationsalgorithmen. Insbesondere verwenden wir die Maximum-Likelihood Klassifikation mit mehreren polarimetrischen und textuellen Indices. Zunächst schlagen wir eine Analyse der polarimetrischen Radar-Daten mit synthetischer Apertur (SAR) entsprechend des Standes der Forschung vor, um das statistische Verhalten dieser Indices zu untersuchen. Dabei berücksichtigen wir folgende statistischen Modelle: Gauss, log-normal, Beta 1, Weibull, Gamma, K, und Fisher. Wir schätzen die Parameter dieser Modelle mit Hilfe von zwei Methoden, nämlich Maximum Likelihood Schätzung (MLE) und Methode der log-Momente (MoLM). Die Wahrscheinlichkeitsdichte der Fisher Verteilung kann alle Deskriptoren ausreichend gut modellieren. Anschließend schlagen wir vor, diese Information in einer angepassten überwachten Klassifizierung auf Basis der Maximum Likelihood und der Fisher-Verteilung zu nutzen. Wir vergleichen die Klassifikationsergebnisse mit jenen aus einer Maximum-Likelihood Klassifikation auf Basis der Wishart- bzw. der Gauss-Verteilung sowie mit jenen aus SVM (Support Vector Machine). Unsere Experimente basieren auf einer Szene im Vorstadtbereich, die mit Hilfe des flugzeuggestützten RAMSES SAR Sensors von ONERA aufgenommen wurde. Unsere Ergebnisse zeigen das Potenzial solcher Daten für die Unterscheidung von urbanen Landbedeckungsarten auf. Die Gesamtgenauigkeit der Klassifikation liegt bei 84%. Allerdings zeigen unsere Ergebnisse auch Probleme, z. B. die häufige Verwechslung von Dächern und Bäumen. Am Ende dieses Beitrages werden mögliche Lösungen für diese Probleme diskutiert.

1 Introduction

In this work, we want to assess the potential of a single polarimetric SAR dataset in a very high spatial resolution context to classify urban land cover classes: different types of roofs, lawn, bare soil, gardens, roads, highways, car parks, playgrounds, trees, shrubs, etc. For that purpose, we concentrate on eight ground classes: *highways* (including roads, parking lots, and concrete playgrounds), *trees* (including also shrubs), *lawn* (which is defined to include bare soil), three kinds of roofs, namely *flat roofs* (defined as non-metallic roofs covered by gravel or concrete that are usually flat), *sloped roofs* (usually covered by tiles) and *metallic roofs* (that can be flat and/or made of periodic structures (see SIMONETTO & MALAK 2009 for examples), *radar shadows* and *bright pixels*.

Using single polarimetric SAR image sets for terrain classification has been a very active field of research work in recent years (LEE et al. 2001, LARDEUX et al. 2007, AINSWORTH et al. 2007, LEE & POTTIER 2009). Some methods are based on the analysis of the physical scattering mechanisms using various polarimetric decomposition theorems, among them (CLOUDE & POTTIER 1997, LEE et al. 2004, LEE et al. 1999, POTTIER & LEE 1999). Other approaches are based on the statistical characteristics of the data or the coherency matrix and derive a decision criterion based on the complex Gaussian or Wishart distributions, as for instance recalled in LEE & POTTIER (2009). In addition, the covariance matrix coupled with a Fisher distributed texture under the scalar product model assumption, can be modeled by a KummerU distribution (BOMBRUN & BEAULIEU 2008). There are also classification algorithms based on image processing techniques, for instance approaches based on the Markovian theory (TISON et al. 2004, FRERY et al. 2007, MOSER et al. 2010), H/A/ α unsupervised classification accompanied by decision trees (SIMONETTO & MALAK 2009) or support vector machines (SVM) (FUKUDA & HIROSAWA 2001, ZHANG et al. 2010).

Here, we assess the performance of different supervised classification methods: SVM and several maximum likelihood (ML) approaches. These processes are applied to a fea-

ture vector composed of amplitudes, co-polarisation ratio, de-polarization ratios, and other polarimetric and textural descriptors.

Initially, particular attention is given to several theoretical and heuristic models for the probability density functions (pdf) of SAR descriptors. This analysis is needed to propose an adapted criterion for a maximum likelihood classification algorithm. As in (SIMONETTO et al. 2002, TISON et al. 2004), the parameters of several parametric statistical distribution models (Gauss, Gamma, Beta 1, Weibull, Log-normal, K, Fisher) are estimated from real data according to different methods. Then the fitting of the estimated models is checked using the K-S (Kolmogorov-Smirnov) test, correlation coefficients and a visual analysis (KRYLOV et al. 2009). Secondly a supervised technique for classification is proposed where an adapted likelihood distance is introduced in a ML framework. In order to assess the performances, the results are compared with those obtained from SVM, ML Wishart classification, and the classical Gaussian-based ML algorithm. The experiments are carried out on a polarimetric image provided by the RAMSES SAR sensor of ONERA, the French Aerospace Lab, over a suburban area.

This paper is structured as follows. The test area and the acquired radar data are presented in section 2, which also includes a short description of the indices used in the feature vector. In section 3, we outline the principle of the statistical analysis and present its results. In section 4, we deal with supervised classification methods and the results achieved by them. Conclusions and perspectives are presented in section 5 of this paper.

2 Studied Area and Dataset

We investigate the potential of X-band fully polarimetric data for discriminating between the principal classes present over a site near Toulouse, France (Fig. 1 a, b). The data are from the ONERA airborne RAMSES (Radar Aéroporté Multi-Spectral d'Etude des Signatures) sensor (DREUILLET et al. 2006). The data is delivered in SLC (single look complex) format, and was acquired in 2006 with an off-nadir viewing angle of 60° and a pixel size of

35 cm in both azimuth and range directions. Because of the large viewing angle, roofs are well represented but not the facades. Besides, these pixel sizes give access to many urban objects and textures on roofs (SIMONETTO & MALAK 2009).

Our main objective is to estimate different urban classes; in particular we are interested in discriminating three types of building roofs: *flat roofs*, *sloped roofs* and *metallic roofs*. *Flat roofs* can be made of different materials such as concrete or gravel, but not of metal. Indeed we do not separate different kinds of flat roofs based on roof material, because it is not possible to distinguish them by image interpretation using both optical and radar views and so it is not possible to build distinct reliable training samples for supervised classification. Indeed, some roofs with the same appearance in the radar image can appear with different colours in the optical view and inversely. In the optical view, they appear in different colours (red, brown and different gray levels) and in the radar data they also show a different appearance (for instance, showing more or less even-bounce or volume-like scattering mechanism). One could work with more roof classes if a ground truth were available to build the training samples. *Sloped roofs* are more likely to be covered by tiles, which are confirmed by their red colour observed in the optical image. The other classes are labelled *lawn*, including lawn and bare soil, *trees* including trees and shrubs, *highways* including roads and car parks, and also two classes, (radar) *shadows* and *bright pixels*. These two last classes do not correspond to any kind of urban objects but

have turned out to be useful to limit the misclassification rate. The *bright pixels* are due to specular phenomena that occur on surfaces that are smooth in comparison to the radar wavelength. They consist of direct and multiple bounces, for instance between the building walls and the ground or between some objects located on a roof and the roof itself. This also happens on point-like objects such as street lights. According to the Rayleigh criterion more bright pixels are expected at larger viewing angles (BECKMAN & SPIZZICHINO 1987).

We define two sets of knowledge: training samples as input in the supervised classification processes and control samples to assess the performance. Training and control data have been extracted manually by visual interpretation of optical views and the radar image (Fig. 1c, d). The training and control data are summarized in Tab. 1.

The fully polarimetric radar system records the complete characterization of the scattering field in all the configurations (HH, VV, HV, VH). Here, we suppose reciprocity with $HV=VH$. The recorded polarimetric data allow a better characterization of the surfaces based on the decomposition theorems. In this work, we use twenty descriptors summarized in Tabs. 2 and 3. In Tab. 2, S_{xy} represents the scattering coefficient of the targets, x the polarization of the incident field, y the polarization of the scattered field, λ_i denotes the i^{th} eigenvalue of the coherency matrix. In the $H/A/\alpha$ decomposition (CLOUDE & POTTIER 1996), the angle α represents the main scattering mechanism (odd-bounce scattering, volume scattering or even-bounce scattering, etc). The

Tab. 1: Training and control samples (numbers of pixels).

Classes	Training data	Control data
Radar shadows	3596	2083
Highways (roads, parks...)	8538	8479
Lawns (lawns, bare soils)	17955	17929
Trees (trees, small shrubs)	4281	3719
Bright pixels	1990	766
Metallic roofs	546	423
Flat roofs	4958	2615
Sloped roofs	235	264

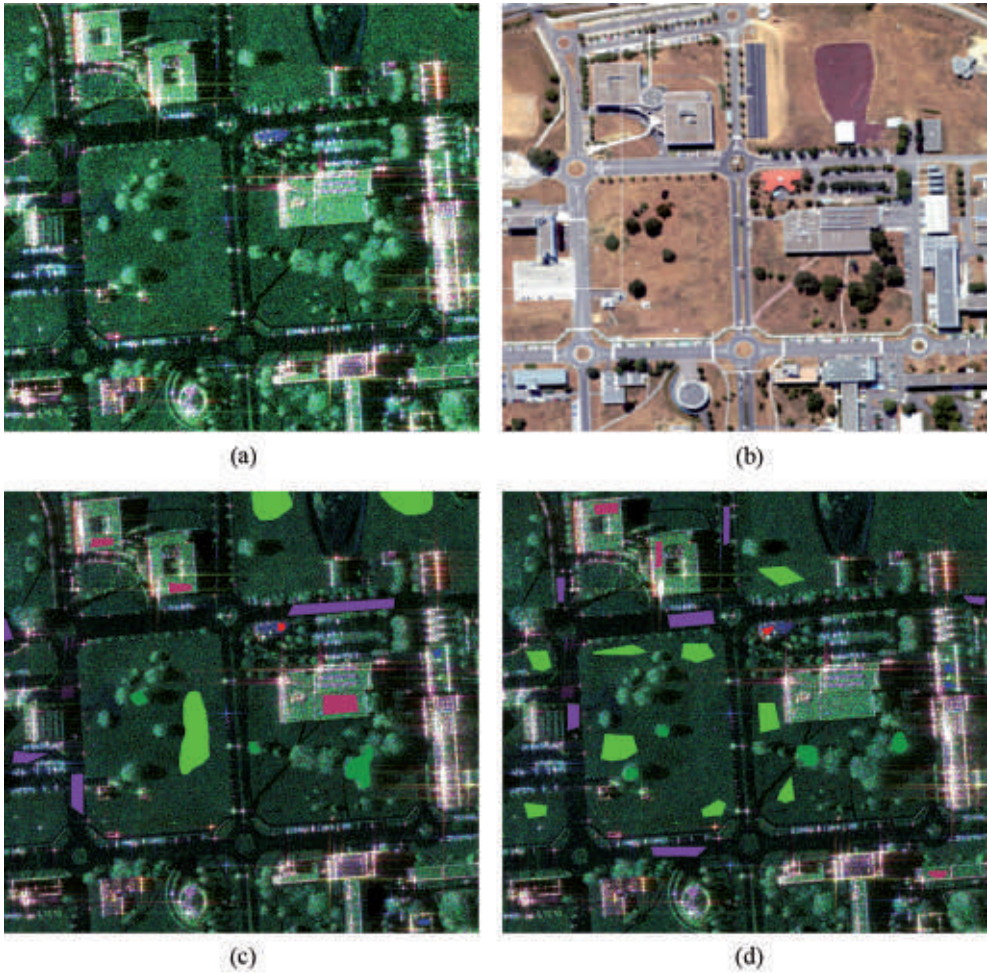


Fig. 1: (a) RAMSES image of the studied site (Toulouse, France), acquired in 2006, in Pauli colour-coded representation, (b) Aerial view from the French Geographical Institute (IGN) acquired in 2006, (c) Training samples superimposed on the RAMSES view (same colour legend as in Fig. 4), (d) Control samples superimposed on the view (same colour legend as in Fig. 4).

entropy H measures the degree of the randomness of the scattering process with the probabilities P_i . The anisotropy A gives the relative importance of the second and third eigenvalues (λ_2 and λ_3 , respectively). We also use the polarization ratios (items 9, 10 and 11 in Tab. 2): the first one is the co-polarization ratio and measures the ratio of the co-polarized signals, S_{HH} and S_{VV} . The other two ratios are e-polarization ratios, $|S_{HV}|/|S_{VH}|$ and $|S_{HV}|/|S_{HH}|$.

As the texture information can be used for improving the classification results (ZHANG et al. 2010), we also include it in our analy-

sis: ENR (energy) gives a measure of textural uniformity, CON (contrast) explains the local variation of grey levels, and HOM (homogeneity) shows the local similarity of the grey values. These statistical parameters are extracted from the grey level co-occurrence matrix (GLCM) (HARALICK 1979) and are summarized in Tab. 3. Each element of this matrix shows the relative frequencies $q(i,j)$ of two neighbouring values that are related to the distance d and angle θ (ZHANG et al. 2010). We arbitrarily choose $d=1$, and $\theta=0^\circ$. Textural parameters are computed on the three images:

Tab. 2: Polarimetric descriptors considered in this work. $\langle \rangle$ stands for the local mean.

No.	Feature	Expression
1	Red Pauli	$ S_{HH} - S_{VV} / \sqrt{2}$
2	Blue Pauli	$ S_{HH} + S_{VV} / \sqrt{2}$
3	Amplitude	$ S_{HH} $
4	Amplitude	$ S_{VV} $
5	Amplitude	$ S_{HV} $
6	Entropy	$H = -\sum_i P_i \log(P_i) = -\frac{\sum_i \lambda_i \log \lambda_i}{\sum_{i=1}^3 \lambda_i}$
7	Anisotropy	$A = (\lambda_2 - \lambda_3) / (\lambda_2 + \lambda_3)$
8	Alpha	$\alpha = \alpha_1 P_1 + \alpha_2 P_2 + \alpha_3 P_3$
9	Co-polarisation ratio	$\langle S_{HH} \rangle / \langle S_{VV} \rangle$
10	De-polarisation ratio	$\langle S_{HV} \rangle / \langle S_{VV} \rangle$
11	De-polarisation ratio	$\langle S_{HV} \rangle / \langle S_{HH} \rangle$

T11, T22 and T33, which are the three diagonal components of coherency matrix T using a 5x5 neighbourhood.

Tab. 3: Mathematical expressions of statistical texture parameters from GLCM. $q(i,j)$: (i,j) th element in the co-occurrence matrix (GLCM = grey level co-occurrence matrix).

Texture parameter	Expression
ENR (energy)	$\sum_{i,j} q(i,j)^2$
CON (contrast)	$\sum_{i,j} i - j ^2 q(i,j)$
HOM (homogeneity)	$\sum_{i,j} \frac{q(i,j)}{1 + i - j }$

3 Statistical Analysis

The precise knowledge of the statistical properties of the SAR data plays a central role in SAR image processing and understanding (GAO 2010). The purpose of this section is to validate a classical statistical model for polarimetric or textural features from our data. This model will then be used in the classification scheme. Besides, this analysis allows us to check the possibility of discriminating each type of land cover according to its statistical behaviour. The process of parametric modelling consists of: (1) selecting several known statistical distribution models; (2) estimating the distribution parameters; (3) assessing the goodness-of-fit of the models.

We select the most widely used distributions in the literature, which are the Gauss, Gamma, Weibull, Beta 1, log-normal, K, and

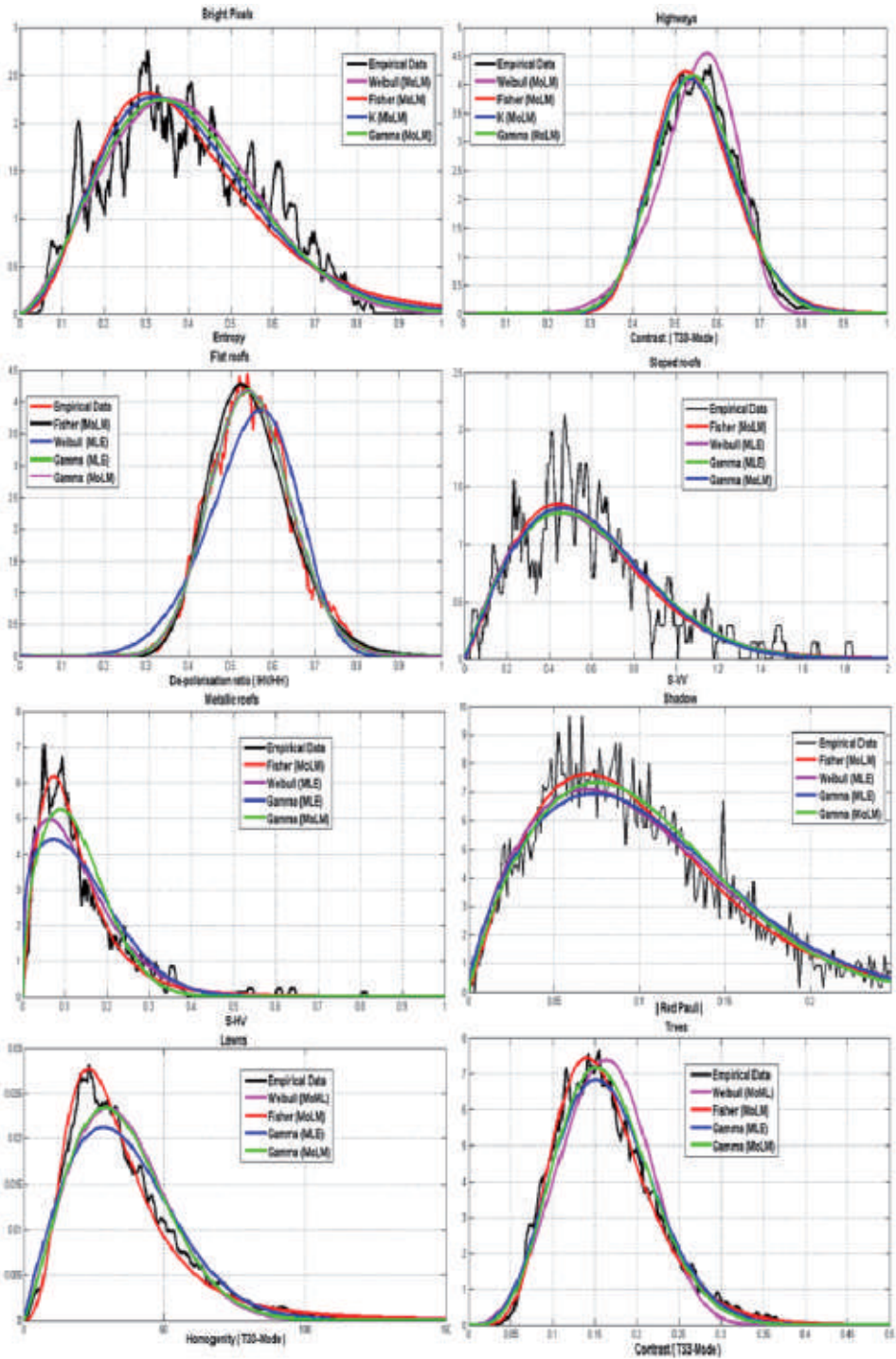


Fig. 2: Empirical data and estimated pdfs using MoLM and MLE for three kinds of roofs, bright pixels, highways, lawns, shadows and trees, and different descriptors (MoLM = method of log-moment, MLE = maximum likelihood estimation).

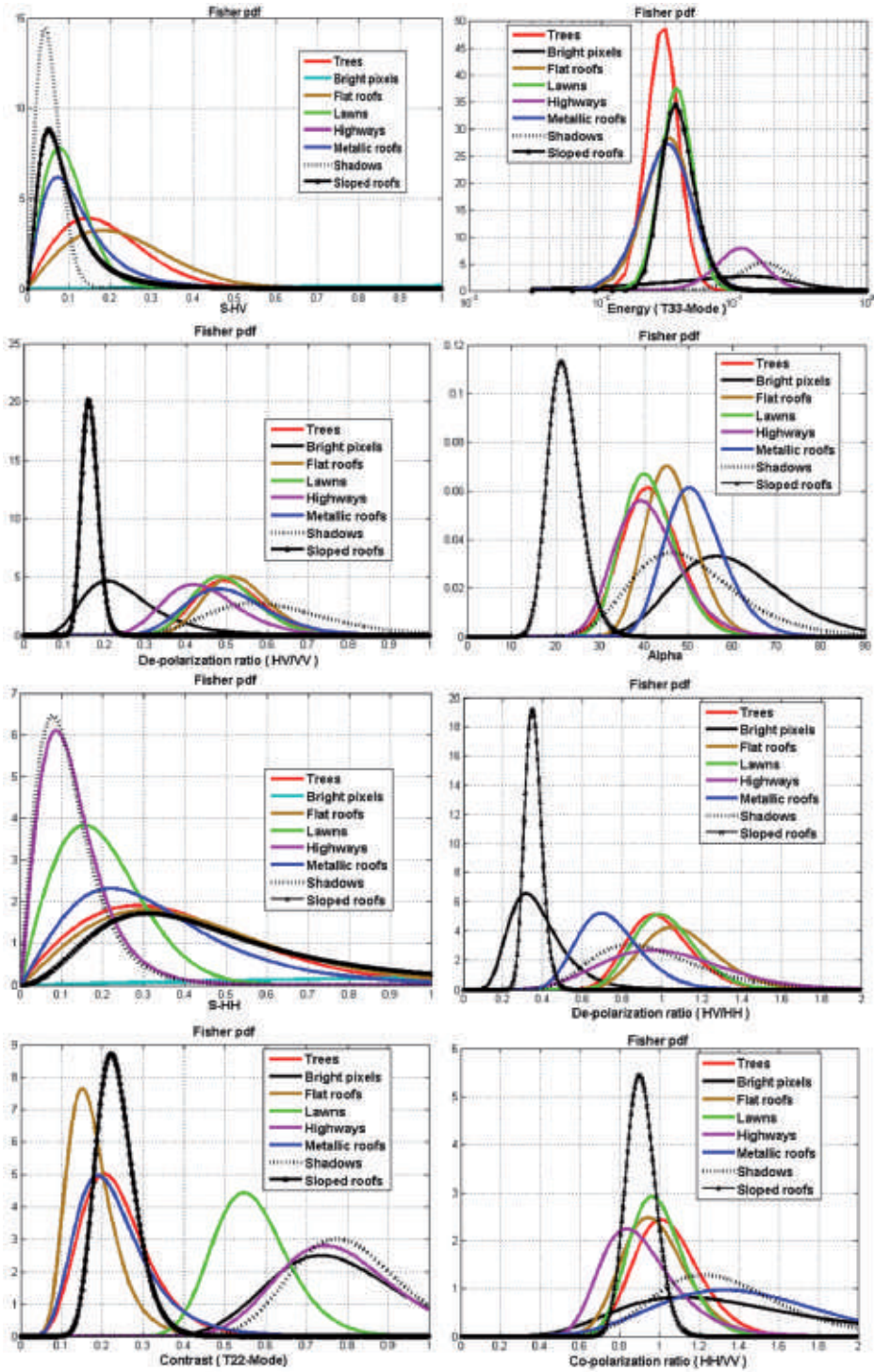


Fig. 3: Estimated Fisher distribution by MoLM for the eight classes and different descriptors.

Fisher distributions. To estimate their parameters, we use two methods: maximum likelihood estimation (MLE), and the method of log-moment (MoLM). We do not use the MLE for K and Fisher pdfs because of mathematical limitations; see NICOLAS (2002) for more details. The MoLM is based on the characteristic function computed on logarithmic scale, from which we obtain parameter estimators from the log-cumulants (NICOLAS 2002, NICOLAS 2006). The formula and algorithm of the Fisher MoML parameter estimation can be found in NICOLAS (2002, page 130). We expect the Fisher distribution to be the more appropriate as it has already been validated for high-resolution SAR amplitude statistics over urban regions (NICOLAS 2006, TISON et al. 2004, BOMBURUN & BEAULIEU 2008).

The GoF (goodness-of-fit) can be assessed by different ways. The K-S (Kolmogorov-Smirnov) hypothesis test involves comparing

the empirical and modelled cumulative distribution functions (FELLER 1948). In this paper, correlation coefficients between empirical and modelled histograms and visual analysis are also used (KRYLOV et al. 2009). During the visual analysis, we represent the empirical and estimated pdfs for each descriptor, each function, each parameter estimation method and each class.

Examples of empirical and modelled histograms are displayed in Fig. 2 for eight descriptors and eight classes. The quantitative results of GoF, obtained with the correlation coefficient and the K-S test for three kinds of roofs and three descriptors are presented in Tab. 4. These comparisons are performed for all descriptors over the eight classes, with all possible parametric functions and both parameter estimation methods.

It turns out that the Fisher pdf is the best model according to the K-S distance or the

Tab. 4: Goodness-of-fit: Correlation coefficients and the K-S (Kolmogorov-Smirnov) distance for three descriptors over three kinds of roofs and for different parametric modelling (MoLM = method of log-moment, MLE = maximum likelihood estimation).

	Sloped roofs and $ S_{VV} $				Metallic roofs and $ S_{HV} $				Flat roofs and De-polarisation ratio ($\langle S_{HV} \rangle / \langle S_{HH} \rangle$)			
	Weibull (MLE)	K (MoLM)	Gamma (MoLM)	Fisher (MoLM)	Weibull (MLE)	K (MoLM)	Gamma (MoLM)	Fisher (MoLM)	Weibull (MLE)	K (MoLM)	Gamma (MoLM)	Fisher (MoLM)
K-S test Distance	0.328	0.3400	0.3433	0.343	0.4160	0.458	0.543	0.316	0.534	0.563	0.566	0.564
Correlation	0.910	0.9142	0.9132	0.915	0.9671	0.985	0.963	0.988	0.974	0.994	0.995	0.992

Tab. 5: Mathematical expressions of the Fisher pdf (for radar amplitude), and the corresponding ML criterion. M, L, μ are the Fisher parameters. $C(i, j)$: Decided class of the pixel (i, j) . N_c : number of classes. N_b : number of features (or bands). $u_b(i, j)$: value of the b^{th} feature of the pixel (i, j) (pdf = probability density function).

Fisher pdf	$p[\mu, L, M](u) = \frac{2\Gamma(M+L)}{\Gamma(M)\Gamma(L)} \sqrt{\frac{L}{M\mu}} \frac{\left(\sqrt{\frac{L}{M\mu}}u\right)^{2L-1}}{\left(1 + \left(\sqrt{\frac{L}{M\mu}}u\right)^2\right)^{L+M}}$
Fisher based ML criterion	$C(i, j) = \arg \max_{k \in [1, N_c]} \left[\sum_{b=1}^{N_b} \log(p[\mu_{k,b}, L_{k,b}, M_{k,b}](u_b(i, j))) - \log N_c \right]$

correlation coefficient. For example the correlation coefficients related to the Red Pauli descriptor of *bright pixels*, are 0.9323, -0.0817, not exist, 0.0688 and 0.8891, respectively, for the following models: Fisher (MoLM), Weibull (MLE), Gamma (MLE), Gamma (MoLM), K (MoLM). The correlation coefficients using the Fisher model are higher, more than 91%, than using the other models, and the K-S distances are smaller (significance level < 5%). This proves the pertinence of the Fisher pdf

that can be retained for all bands and all classes using the MoLM. As a result, the Fisher pdfs for each of the eight classes and for different descriptors are shown in Fig. 3.

Besides, such analysis confirms the existence of clear different statistical behaviours such as between *bright pixels* and *highways* using a de-polarization ratio, or between *highways* and *shadows* using the co-polarization ratio.

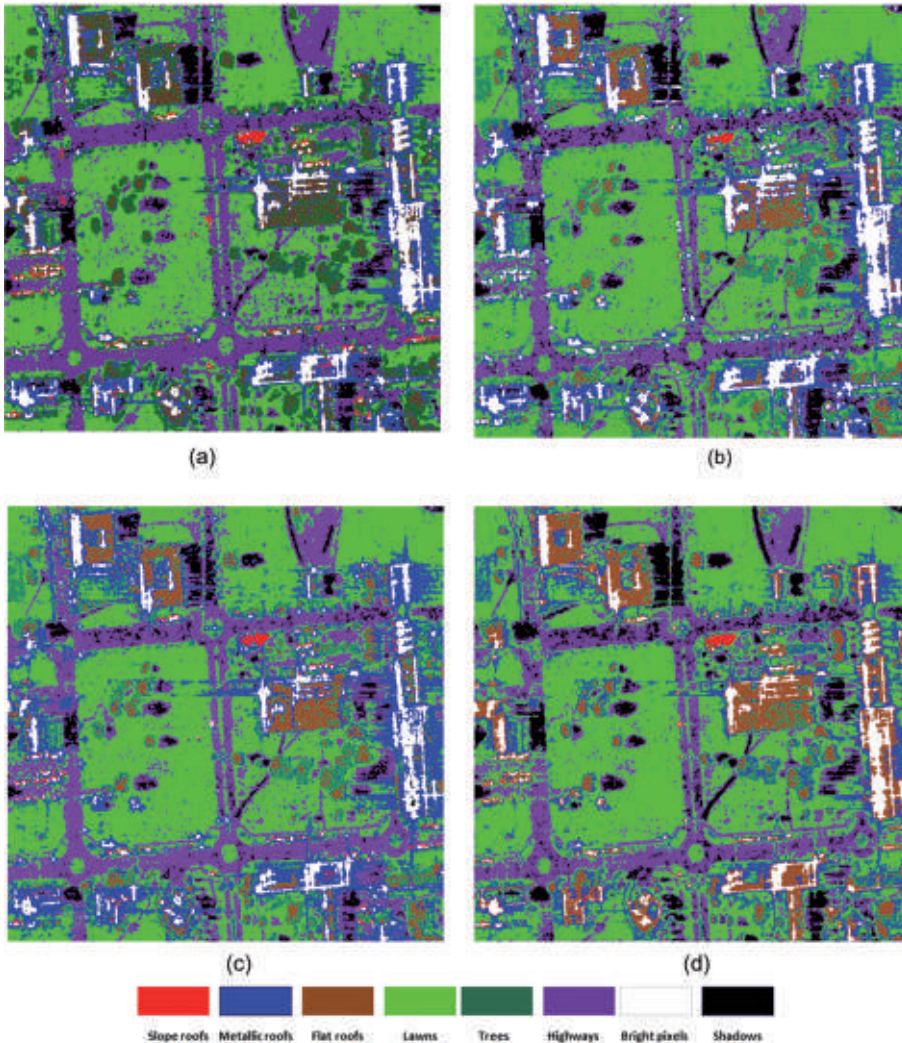


Fig. 4: Classification result: (a) SVM * (b) G-ML * (c) F-ML * (d) W-ML. * is for classification using 20 bands (11 polarimetric descriptors and 9 textural ones, SVM = support vector machine, G-ML = circular Gaussian-based, F-ML = Fisher-based, W-ML = Complex Wishart, ML = Maximum likelihood classification).

Some classification results from the different approaches are shown in Fig. 4. Tab. 6 gives the performance of the different tests with and without the textural information. The performance is presented in the different columns of this table: “rate of good classification for each class” (in columns 2 to 9), “kappa coefficient” that is the Cohen’s Kappa computed in ENVI (in column 10) and “overall accuracy” defined by the rate of good classification (producer’s accuracy) (in column 11).

In this table, we observe that *shadows* and *bright pixels* are better classified with the G-ML using 20 bands. Indeed, the Fisher pdf is the best modelling for each feature according to the analysis in section 3 but our F-ML criterion does not take into account the band statistical dependency, which could explain this result. Despite this limitation, the F-ML using 20 bands leads to the best producer’s accuracy for the class *flat roofs*. SVM with 20 bands is preferable for *highways*, *lawns* and *trees*. The classification of sloped roof pixels is better with SVM or F-ML without using the textural descriptors. Note that the image shows only one sloped roof and the training and control samples for this class are smaller than for the other classes. The best result for *metallic roofs* is obtained with SVM without using the textural descriptors.

We can state that using the texture properties such as uniformity, contrast, and homogeneity, the overall accuracy result for all three classification methods is greatly improved; for SVM from 64.4% to 84.5%, G-ML from 65.7% to 80.6%, and F-ML from 64.2% to 80.7% (Tab. 6).

Indeed, the producer’s accuracies have increased for most classes.

This is not the case for the classes *metallic roofs*, *shadows* and *sloped roofs* (Tab. 6). If we observe the complete confusion matrices (Tab. 7 for an example), the confusion between *shadows* and *highways*, and between *metallic roofs* and *flat roofs* and *trees*, are more important in the results when using the textural descriptors (that is, 20 bands).

On the other hand, certain rates of misclassification have been reduced. This is the case for *trees*, for which two main classification errors are caused by a confusion with *flat roofs* and *lawns*. Using the F-ML, the confusion with

lawns is reduced from 20.6% to 5.9% (Tab. 7). However, the confusion with *flat roofs* is increased from 31.4% to 37.3%. The same tendency is observed using the G-ML algorithm. Similarly, *flat roofs* are confused with the class *trees*. The rates of confusion of *flat roof* pixels that are erroneously classified as *trees* using textural descriptors are equal to 21.2% with F-ML, 31.8% with G-ML and 30.0% with SVM. Then, the best result is obtained with the F-ML approach for *flat roofs*. In the same way, the *lawn* is less frequently confused with *highways* and *trees* if the textural bands are used.

To conclude this analysis, the textural features are relevant to the classification process for most classes. Although we do not obtain the best classification accuracy with the F-ML algorithm, it allows for a better discrimination of *lawns* and *flat roofs*. However, the results obtained for *metallic roofs* with this criterion are quite poor.

5 Conclusions and Perspectives

This paper has presented a validation of the Fisher pdf to model twenty polarimetric and textural descriptors and proposed a new supervised ML classification based on the Fisher pdf. The result is compared with several supervised classification results (SVM, ML based on a Gaussian pdf, Complex Wishart ML algorithm).

The overall classification accuracy using twenty bands obtained from the F-ML classification is 81% and Cohen’s Kappa is equal to 0.72. Although the Fisher ML criterion does not show the best overall accuracy compared to other classifiers, the classification results obtained by F-ML have a less noisy visual appearance, and the algorithm appears to be more efficient than SVM, W-ML or G-ML to discriminate flat roofs from trees. Introducing textural features allows us to greatly increase the overall accuracy of the classification process. Nevertheless, misclassifications still occur between flat roofs and trees and for metallic roofs.

This result could be considered poor compared to those that one can obtain using an optical data. However, a first work has shown that the classified radar image provides infor-

mation that is complementary to a classified spectral image (LONG et al. 2010). For example, the radar data allows to separate road surfaces from flat roofs which was not the case with the spectral data.

As a suggestion for future work, a comparison with the KummerU-distribution based classification (BOMBRUN & BEAULIEU 2008) would be interesting. We will study a new Fisher ML criterion that takes into account the statistical dependencies between features. Besides, we think that contextual information is necessary to properly discriminate different kinds of roofs and to overcome the confusion between some kind of roofs and trees. Contextual information could be other radar images (with a different wavelength), spectral data, or geometric information (shape or elevation). These topics may be investigated in future studies.

Acknowledgements

We thank ONERA/DEMR for providing the RAMSES data.

References

- AINSWORTH, T.L., LEE, J.-S. & CHANG, L.W., 2007: Classification comparisons between dual-pol, compact polarimetric and quad-pol SAR imagery. – IEEE IGARSS: 164–167.
- BECKMAN, P. & SPIZZICHINO, A., 1987: The scattering of electromagnetic waves from rough surfaces. – 512 p., Artech House Radar Library, Norwood, Massachusetts, USA.
- BOMBRUN, L. & BEAULIEU, J.M., 2008: Fisher Distribution for Texture Modeling of Polarimetric SAR Data. – IEEE Geoscience and Remote Sensing Letters **5** (3): 512–516.
- CLOUDE, S.R. & POTTIER, E., 1996: A Review of Target Decomposition Theorems in Radar Polarimetry. – IEEE TGRS **34** (2): 498–518.
- CLOUDE, S.R. & POTTIER, E., 1997: An entropy based classification scheme for land applications of polarimetric SAR. – IEEE TGRS **35** (1): 68–78.
- Dreuillet, P., Cantalloube, H., Colin, E., Dubois-Fernandez, P., Dupuis, X., Fromage, P., Garestier, F., Heuze, D., Oriot, H., Peron, J.L., Peyret, J., Bonin, G., Du Plessis, O.R., Nouvel, J.F. & Vaizan, B., 2006: The ONERA RAMSES SAR-latest significant results and future developments. – IEEE Conf. Radar: 2046–2057.
- FELLER, W., 1948: On the Kolmogorov-Smirnov Limit Theorems for Empirical Distributions. – Annals Mathematical Statistics **19** (2): 177–189.
- FRERY, A.C., CORREIA, A.H. & DA FREITAS, C.D., 2007: Classifying Multifrequency Fully Polarimetric Imagery With Multiple Sources of Statistical Evidence and Contextual Information. – IEEE TGRS **45** (10): 3098–3109.
- FUKUDA, S. & HIROSAWA, H., 2001: Support vector machine classification of land cover: application to polarimetric SAR data. – IEEE IGARSS: 187–189.
- GAO, G., 2010: Statistical Modeling of SAR Images: A Survey. – Sensors **10** (1): 775–795.
- HARALICK, R.M., 1979: Statistical and structural approaches to texture. – Proceedings of the IEEE **67** (5): 786–804.
- KRYLOV, V., MOSER, G., SERPICO, S.B. & ZERUBIA, J., 2009: Modeling the statistics of high resolution SAR images. – INRIA-00342681.
- LARDEUX, C., FRISON, P.-L., TISON, C., DELEFLIE, D., SOUYRIS, J.-C., RUDANT, J.-P. & STOLL, B., 2007: Comparison of Compact Polarimetric with Full Polarimetric Radar Data for Land Use Discrimination Based on SVM. – POLinSAR, Frascati, Italy.
- LEE, J.S., GRUNES, M.R., AINSWORTH, T.L., DU, L.J., SCHULER, D.L. & CLOUDE, S.R., 1999: Unsupervised Classification using Polarimetric Decomposition and the Complex Wishart classifier. – IEEE TGRS **37** (5): 2249–2259.
- LEE, J.S., GRUNES, M.R. & POTTIER, E., 2001: Quantitative Comparison of Classification Capability – Fully Polarimetric versus Multipolarisation SAR. – IEEE TGRS **39** (1): 2343–2351.
- LEE, J.S., GRUNES, M.R., POTTIER, E. & FERROFAMIL, L., 2004: Unsupervised terrain classification preserving scattering characteristics. – IEEE TGRS **42** (4): 722–731.
- LEE, J.S. & POTTIER, E., 2009: Polarimetric Radar Imaging: From Basics to Applications. – Optical Science and Engineering, B.J. Thompson, New York.
- LONG, N., SIMONETTO, E. & BOCHER, E., 2010: A combined approach to detect urban features from multi-spectral and radar data. – IEEE IGARSS: 1469–1472.
- MOSER, G., KRYLOV, V., SERPICO, S.B. & ZERUBIA, J., 2010: High-resolution SAR-image classification by Markov random fields and finite mixtures. – SPIE Computational Imaging, doi:10.1117/12.838594.
- NICOLAS, J.-M., 2002: Introduction aux statistiques de deuxième espèce: Application des logs-moments et des logs-cumulants à l'analyse des lois

- d'images radar. – *Traitement du Signal* **19** (3): 139–167.
- NICOLAS, J.-M., 2006: Application de la transformée de Mellin: Etude des lois statistiques de l'imagerie cohérente. – ENST, Paris, France.
- POTTIER, E. & LEE, J.S., 1999: Application of the H/A/ α Polarimetric Decomposition Classification of fully polarimetric SAR data based on the Wishart Distribution. – CEOS SAR Workshop, ES-SP 450: 335–340.
- RICHARDS, J.A., 1999: Remote Sensing Digital Image Analysis. – 240, Springer-Verlag, Berlin.
- SIMONETTO, E., ORIOT, H. & GARELLO, R., 2002: Extraction of industrial buildings from stereoscopic airborne radar images. – *SPIE Remote Sensing* **4543**: 121–129.
- SIMONETTO, E. & MALAK, C., 2009: Urban area structuring mapping using an airborne polarimetric SAR image. – *SPIE Remote Sensing* **7477**: 74771X.
- TISON, C., NICOLAS, J.-M., TUPIN, F. & MAÎTRE, H., 2004: A new statistical model for Markovian classification of urban areas in high resolution SAR images. – *IEEE TGRS* **42** (10): 2046–2057.
- WU, T., LIN, C.-J. & WENG, R.C., 2004: Probability estimates for multi-class classification by pairwise coupling. – *Journal of Machine Learning Research* **5**: 975–1005.
- ZHANG, L., ZOU, B., ZHANG, J. & ZHANG, Y., 2010: Classification of Polarimetric SAR Image Based on Support Vector Machine Using Multiple-Component Scattering Model and Texture Features. – *EURASIP Journal on Advance in Signal Processing* **2010**: 21–29.

Address of the Authors:

MARYAM SOHEILI MAJD, ELISABETH SIMONETTO and LAURENT POLIDORI, L2G, ESGT, 1 Bd Pythagore, 72000 Le Mans, France, Tel.: +33-2-4343-3100, Fax: +33-2-4343-3102, e-mail: {maryam.soheili_majd}{elisabeth.simonetto}{laurent.polidori}@esgt.cnam.fr

Manuskript eingereicht: Oktober 2011

Angenommen: Mai 2012